# Dorso-ventral hippocampal neural assemblies are preferentially reactivated during NREM sleep following an aversive experience

Morici JF[1], Paiva-Lima I[1], Pronier É[1], Girardeau G[1,*]

1Institut du Fer à Moulin, Inserm U1270, Sorbonne Université, Paris

*corresponding author: gabrielle.girardeau@inserm.fr

## Abstract

Sleep plays a crucial role in memory stabilization. In the dorsal hippocampus (dHPC), fast oscillations (sharp-wave ripples) during non-REM sleep consolidate spatial memories through place cell reactivation. The hippocampal formation is heterogeneous; the dHPC processes mostly contextual information, while the ventral part (vHPC) encodes valence and anxiety. We propose that dorsal-ventral communication during sleep is involved in the consolidation of emotional memories, potentially integrating or segregating contextual and valence information. To test this, we recorded the electrophysiological activity in the dHPC and vHPC in rats during reward and aversion-motivated exploration of a linear track and subsequent sleep. We detected dorsal and ventral SWRs during NREM sleep as well as neuronal assemblies during each exploration type and identified dorsal, ventral, and joint (dorso-ventral) assemblies. We found that dorso-ventral hippocampal coordination involves coordinated ripples and bursts of ripples. Aversive joint assemblies exhibited higher reactivation during non-REM sleep than the joint assemblies from the reward condition. Interestingly, joint aversive assemblies reactivated selectively during dorso-ventral coordinated ripples. Furthermore, their reactivation strength positively correlated with their strength of activation during the task. These results suggest the existence of dorsal-ventral hippocampal functional communication capable of sustaining the selective reactivation of experiences based on their emotional valence.

## Introduction

Episodic memory is supported by the hippocampus, a heterogeneous brain structure with distinct functional and anatomical properties along its dorsoventral axis (Fanselow and Dong 2010; Bannerman et al. 2004; Strange et al. 2014). The dorsal hippocampus (dHPC) encodes spatial representations of the environment through the activity of place cells, which code for specific locations called place fields (O'Keefe 1976; M. a Wilson and McNaughton 1993). During NREM sleep (slow-wave sleep), these spatial representations are reactivated (M. A. Wilson and McNaughton 1994; Skaggs and McNaughton 1996), preferentially during fast oscillatory hippocampal events known as "sharp-wave ripples" (SWRs) (Buzsáki 2015). Dorsal SWRs support spatial (Gabrielle Girardeau et al. 2009; Ego-Stengel and Wilson 2009) and contextual fear (Wang et al. 2015) memory consolidation. Interestingly, dHPC spatial representations can be modulated by the emotional valence of the environment, notably through remapping (Moita et al. 2004; D. V. Wang et al. 2015; Schuette et al. 2020; Hollup et al. 2001; Dupret et al. 2010). Moreover, dHPC sleep reactivations after an aversive experience can occur conjointly with the basolateral amygdala (BLA) (G. Girardeau, Inema, and Buzsáki 2017), which is involved in fear processing, and other emotion-processing structures (Lansink et al. 2008; 2009; Pennartz et al. 2009). However, the dHPC has no direct anatomical connections with the BLA and only marginal ones with the rest of the emotional network, including the mPFC, nucleus Accumbens and VTA (Malik et al. 2022; Harvey et al. 2023).

Compared to the dHPC, the ventral hippocampus (vHPC) is understudied, particularly regarding its role in memory consolidation during sleep (Pronier, n.d.). The vHPC displays poorer spatial coding properties than the dHPC (Jung, Wiener, and McNaughton 1994; Kjelstrup et al. 2008), but plays a stronger role in emotional processing, particularly in anxiety-like behaviors (Forro et al. 2022; Jimenez et al. 2018; Ciocchi et al. 2015) and fear processing (Jimenez et al. 2020; Herbst, Twining, and Gilmartin 2022). Unlike the dHPC, the vHPC has reciprocal anatomical connections with the emotion-processing network, such as the BLA (Pitkänen et al. 2000; Binder et al. 2019). The vHPC is necessary for contextual fear memory consolidation during sleep, notably through its connections with the BLA (Huff et al. 2016; G.-W. Wang, Liu, and Wang 2017). Therefore, the vHPC could serve as a relay structure to integrate the contextual and spatial information being reactivated in the dHPC with the emotional valence processed in the vHPC and BLA. To date, only one study has reported

reactivations implicating the vHPC following fear conditioning (Miyawaki and Mizuseki 2022), conjointly with the BLA, associated with SWR events.

SWRs propagate along the dorsoventral axis of the hippocampus, and marginal coordination of those events between dorsal and ventral parts has been reported during sleep without prior learning or emotional experience (Patel et al. 2013). We hypothesize that changes in the coordination of dorsal and ventral hippocampal ripples could foster the reactivation of joint dorso-ventral neuronal assemblies encoding the spatial and emotional components of an experience. To study the respective and conjoint roles of the dHPC and the vHPC in the sleep-dependent processing of emotionally valenced experiences, we recorded neuronal activity in both regions simultaneously in rats performing a new task specifically designed to elicit the same behavior in the same spatial environments, but with opposing valences. These rats were subjected to aversive or reward-motivated exploration on a linear track, preceded and followed by sleep periods. We identified dorsal, ventral, and dorsoventral joint cell assemblies in the hippocampus that represented the aversive and reward conditions of the task. We then investigated whether those assemblies were reactivated during subsequent NREM sleep, the extent to which they coincide with the dorsoventral coordination of SWRs, and how these were influenced by emotional valence.

# Results

## Rats can perform the same exploratory behavior motivated by either reward or avoidance.

To study dorsal-ventral hippocampal joint reactivations, we developed a behavioral task where animals have to perform the same exploratory behavior on a linear track but under different motivational contingencies associated with opposite valences. In the reward-motivated, positive contingency, the rats have to run back and forth on the linear track to obtain a drop of water at the end of each lap (Rewarded Run). The avoidance-motivated, aversive contingency was conducted on the same linear track and signaled by a single, constant light cue. During this session, animals were running back and forth to avoid an eyelid shock (Aversive Run) delivered after 20-30 seconds of immobility. (**Figure 1A-B**). During pre-training, the animals very rapidly learned to alternate for

rewards, but the shock condition had to be gradually introduced to preserve the mobility and alternation behavior (**Figure S1A**). The experiments started at plateau performance for the number of shocks. The beginning of the plateau performance was defined as a drop in the number of shocks by at least 50% (**Figure 1B**, lower panel, session 0). The number of rewarded laps, but also the number of aversive laps and shocks remained stable across all subsequent recording sessions (**Figure 1B**, upper and middle panels). Each day, animals performed both the reward and aversive version of the task, preceded and followed by 2 to 3 hours of rest in their homecage. The order of the reward and aversive runs was switched every day. Despite a decrease in global speed during aversive runs compared to reward ones (**Figure S1C**), animals explore homogeneously the linear track in both, aversive and rewarded runs (**Figure S1B**) and the speed distribution patterns across space are similar (**Figure S2A**). To pair the behavior across conditions, we selected moments in which animals were either active or quiet. We did not find significant differences in occupancy in either of these states across space (**Figure S2B-C**) or in total time between conditions (**Figure S2C**).

## Dorsal-ventral coordinated ripples occur in bursts.

We recorded local field potentials and neuronal ensembles from the dorsal and ventral CA1 hippocampal regions (**Figure S3**) in a total of 47 sessions (5 rats with simultaneous dHPC and vHPC recordings; 1 rat vHPC). Each unit was categorized as putative pyramidal cells (Pyr) or putative interneurons (Int) (see Methods). We identified a total of 1,615 units in both structures. A total of 544 units were from the vHPC (pyr: 461; int: 83) and 1071 from the dHPC (pyr: 856; int: 215). The firing rate was higher in putative interneurons compared to putative pyramidal cells within both regions (**Figure S4**). Putative pyramidal cells in the dHPC exhibited a higher burst index, consistent with the existing literature (Connor & Gutnick, 1990). Sharp-wave ripple complexes (SWRs) in the dHPC and vHPC were detected by thresholding the normalized square root of the filtered local-field potential (**Figure 2A, B**). We found that dorsal ripple rates were significantly higher than ventral ones (**Figure 2C**). Dorsal ripple rate, but not ventral ripple rate increased during sleep following either the rewarded or the aversive session, compared to baseline sleep (**Figure S6A**). Moreover, we did not observe changes in the autocorrelograms of dorsal or ventral ripples, even when separated by emotional valence (**Figures S6B-C**).

Dorsal and ventral ripples were shown to be partially coordinated (Patel et al. 2013) during NREM sleep, but it is yet unknown how spatial exploration or an emotional experience might affect this coordination during subsequent sleep. On the cross-correlation between dorsal and ventral ripples, the central peak was shifted to positive time bins, suggesting that ventral ripples tend to occur after dorsal ones (**Figure 2D**). The existence of 2 additional peaks within a +-100ms window suggests that dorso-ventral coordination occurs through bursts of ripples. Based on this temporal coordination, we defined coordinated events as events during which a dorsal ripple occurred within 100 ms of a ventral one. Both dorsal and ventral ripples showed a percentage of coordinated events significantly higher than chance (**Figure 2E**). The proportion of coordinated events was not increased after either valenced exploration compared to baseline (**Figure S6D**). The amplitude of coordinated dorsal and ventral ripples was higher than the amplitude of uncoordinated ripples (**Figure S6E**), as reported previously (Patel et al. 2013). This did not affect the recruitment of single units by dorsal or ventral ripples, which does not differ between coordinated and uncoordinated ripples (**Figure S6F**). Finally, we found that in both dorsal and ventral hippocampus, coordinated ripples tend to occur in bursts compared to uncoordinated ripples, as indicated by the different peaks on the coordinated x uncoordinated cross-correlagrams and the burst index (**Figure 2F,G**).

## Dorsal bursts occur preferentially before ventral ones.

We aimed to explore whether communication between the dorsal and ventral hippocampus could be mediated by coordinated ripple bursts, and if so, whether one region may lead to the coordination. Using cross-correlations between coordinated and uncoordinated ripples in the dorsal and ventral HPC, we found that in the dorsal hippocampus, uncoordinated events tend to occur before coordinated ones, whereas in the ventral hippocampus, this tendency was reversed (**Figure 2H**). These results suggest that dorsal-ventral coordination might occur at the end of a dorsal burst and the beginning of a ventral burst. To test this hypothesis, we detected ripple bursts in both regions by identifying sequences of ripples occurring within less than 100 milliseconds of each other (**Figure S7A**). We found that burst durations were not different between structures (**Figure S7B**), showing a temporal dorsal-ventral overlap of ≈100 ms (**Figure S7C**). Next, we aimed to determine if one of the two structures was leading the burst coordination. We first constructed a histogram of the time

differences between the end of dorsal ripple bursts and the beginning of ventral ones. We observed a probability peak between 0-500 ms, suggesting that dorsal ripples tend to end after ventral ones have started (**Figure 2I**). Additionally, we constructed a peri-event histogram of the starting times of dorsal bursts aligned to the end of ventral bursts. Consistent with our previous analysis, we found that dorsal ripple bursts tend to start before the end of ventral ones (**Figure 2J**). Experience also modulates ripple burstiness, with both aversive and rewarded conditions leading to an increase in the proportion of ripples occurring in bursts in the dorsal, but not the ventral hippocampus (**Figure S7D**). Overall, these results show that dorso-ventral coordination occurs at the level of single ripples but also ripple bursts, with the dorsal hippocampus leading the ventral hippocampus. Experience might modulate coordination at both these scales.

## Dorsal-ventral joint assemblies better disambiguate the reward and aversive conditions

Next, we examined the changes in dorso-ventral coordination at the level of neuronal assemblies. Neuronal assemblies were detected using a PCA-ICA method (Lopes-dos-Santos, Ribeiro, and Tort 2013)**(Figure S8**) either during the aversive or the rewarded condition on all simultaneously recorded pyramidal neurons in the dorsal and ventral hippocampus. The detection was restricted to moments of behavioral activity (**Figure S2C**). For each of the 446 detected assemblies, we applied a threshold to the ICA weight vectors to determine the neurons that were significantly contributing to the assembly (**Figure 3A**). We differentiated 277 assemblies with only dorsal hippocampus contributing members (131 aversive and 146 rewarded), 62 assemblies with only ventral hippocampus members (37 aversive and 25 rewarded), and 107 assemblies with contributing members from both the dorsal and ventral hippocampus. We called these joint assemblies (54 aversive and 53 rewarded). We did not detect differences in the number (**Figure S9A**) or proportions (**Figure S9B**) of members across assembly types (dorsal, ventral, or joint). Assemblies were separately detected on the same set of neurons during either the aversive or the reward conditions. Comparing the overlap between assemblies detected in the aversive vs. the reward condition is indicative of the difference in the neural representation of similar environments with different contextual valences. We computed the similarity index across pairs of dorsal, ventral, or joint assemblies detected in different valence

conditions and detected significantly similar pairs (**Figure 3B**). Joint assemblies showed less overlapping between the aversive and rewarded conditions compared to the other two types of assemblies (**Figure 3C**). This result suggests that the contextual valence is better disambiguated by representations involving both the dorsal and ventral neurons.

## Aversive joint assemblies reactivate more during the following NREM sleep than joint reward assemblies

During sleep after an experience, neuronal assemblies formed and activated during the exploration show an increased reactivation pattern in the dorsal hippocampus (M. A. Wilson and McNaughton 1994; van de Ven et al. 2016) and also between the dorsal hippocampus and basolateral amygdala (G. Girardeau, Inema, and Buzsáki 2017). However, it remains unclear if those patterns of assembly reactivation occur along the dorsal-ventral hippocampal axis and if a potential modulation exists based on the emotional valence of the awake experience. To address this, we calculated the strength of activation for each joint assembly detected during the aversive or reward experience during the rest of the recording session, including REM and NREM sleep in the homecage (**Figure 3D**). Then we calculated the rate of peaks of activation (see Methods) in 60-second bins during NREM sleep before and after the rewarded or aversive exploration (**Figure 4A**). Both aversive and reward joint assemblies exhibited higher activation rates during post-sleep compared to pre-sleep periods. This difference diminishes over the course of the sleep session (0-20 minutes vs 20-40 minutes of NREM sleep; **Figure 4B**), consistent with previous observations that reactivations rapidly decline over the first hour of NREM sleep (G. Girardeau, Inema, and Buzsáki 2017; Miyawaki and Mizuseki 2022). The same result was observed for dorsal and ventral assemblies (**Figure S10**). Interestingly, the activation rates of the joint assemblies during sleep following the aversive experience were also significantly higher than following the rewarded experience (0-20min: $p_{KS}$=9,97x$10^{-6}$; 20-40min: $p_{KS}$=0.83). This increased reactivation after the aversive cognition was not observed for dorsal or ventral assemblies only. To confirm this observation, we computed the peak reactivation strength (see Methods), which reflects the magnitude of the detected peaks during post-sleep controlled for the magnitude observed during pre-sleep. Again, we observed a significantly higher reactivation for the joint aversive assemblies compared to the reward joint assemblies (**Figure 4C**). Then we wanted to test whether

this increased reactivation was initiated during the exploration of the track. We found that the reactivation strength positively correlated with the strength of the assemblies during the exploration of the aversive, but not the rewarded condition (**Figure 4C-D**). This correlation was selective for joint aversive assemblies, and not present for either joint reward assemblies or dHPC/vHPC assemblies in either condition (**Figure S11**). No differences in activation rates nor reactivation strength were found for any of the assembly types during REM sleep (**Figure S12** ). These results indicate that the exploration of a given environment under aversive conditions selectively recruits assemblies spanning both the dorsal and ventral hippocampus that will be later reactivated during sleep.

## The reactivation strength of joint aversive assemblies is increased during dorsal-ventral coordinated ripples.

Assembly pattern reactivations have consistently been found to co-occur with ripple oscillations (Diba and Buzsáki 2007; Foster and Wilson 2006), and later on in ripple burst events (Davidson, Kloosterman, and Wilson 2009). Since ripple oscillations have been shown to synchronize the activity of long-distance structures, they might represent a time window instrumental for the hippocampus to transfer information coded during wakefulness. We thus tested whether the observed reactivations of the joint assemblies were specifically occurring during coordinated ripple events. We calculated the Peak Reactivation Strength, during dorsal-ventral coordinated and uncoordinated ripple events. We found that only joint aversive, but not reward, assemblies showed a significant increase in peak reactivation strength during dorsal-ventral coordinated events (**Figure 5**, left). This result was not observed for dorsal or ventral aversive assemblies (**Figure S13A**). Although there was a slight increase in joint aversive assembly reactivation during uncoordinated ventral ripples, the increase in Peak Reactivation Strength for joint aversive assemblies was mostly selective for dorsal-ventral coordinated ripples (**Figure 5**, middle, right). Dorsal or ventral assemblies did not show any increase relative to uncoordinated or coordinated ripples (**Figure S13B-C**). These results indicate that dorso-ventral coordinated ripples constitute a permissive time window for the reinstatement of the representation of an aversive environment by the joint neural activity of the dorsal and ventral hippocampus.

## Discussion

This study examined dorsal-ventral hippocampal coordination at both population and single-unit levels during awake experiences of reward and aversive spatial navigation, as well as during subsequent sleep processing. We found that temporally coordinated dorsal and ventral ripples tended to occur in bursts, with dorsal ripples leading ventral ripples. We identified dorsal and ventral hippocampal assemblies as well as dorsoventral joint assemblies during both types of emotional experiences, with joint assemblies showing less similarity overlap between emotional conditions. Reactivation of assemblies during NREM sleep was observed for all assembly types, with higher intensity for joint aversive assemblies, particularly during coordinated dorsal and ventral ripples.

Ripple occurrences in the dorsal hippocampus have been previously shown to be up-modulated by previous exposition to a learning task (O'Neill et al. 2010). Similarly, we found that both aversive and rewarded run sessions trigger the increase of ripple rate compared to baseline sleep in the dorsal hippocampus (**Figure S6A**). However, in the ventral hippocampus, we found that neither the rewarded nor aversive experience triggered an increase in ripple rate during subsequent NREM sleep compared to baseline. In addition to rate changes, the aversive or rewarded experiences also trigger an increase in burstiness, i.e. the tendency for ripples to occur in groups of 2 or more, in the dHPC, but not in the vHPC. Bursts of SWRs in the dHPC have been previously reported to promote extended replay sequences of experiences in large environments (Davidson, Kloosterman, and Wilson 2009). This suggests that the synchronized activity between dHPC and vHPC for the processing of complex contextual-emotional experiences could be facilitated by coordinated bursts of SWRs. A subset of ripples are coordinated across the dorso-ventral axis of the hippocampus in baseline conditions (Patel et al. 2013). Here, we show that this coordination also exists during sleep following spatial navigation under different valences. Indeed, a subset of ripples are coordinated, thanks to an overlap in bursts of ripples initiated in the dorsal hippocampus and finishing in the vHPC.

Previously published studies on cross-structure reactivations similarly showed that the dHPC tends to lead the reactivations (Lansink et al. 2008; 2009; Pennartz et al. 2009). This sequential activation may reflect a process where spatial information from the dHPC is processed first, followed by emotional and contextual information from the vHPC. Surprisingly, and despite an increase in rate and burstiness in the dHPC, neither an aversive nor positive experience triggers a change in dorso-ventral

255 ripple coordination (**Figure S2D**). This suggests the existence of more subtle modifications at the level
256 of neuronal assemblies.

257 Cell assemblies with synchronously active neurons from both the dorsal and ventral hippocampus
258 neurons were shown to develop during the exposition to contextual fear conditioning (Pompili, Hamou,
259 and Wiener 2024). Here, we detected dorsal, ventral, and dorso-ventral joint assemblies during
260 aversive-motivated and rewarded-motivated exploration using the same set of neurons (**Figure 3A-**
261 **B**). When examining the overlap between the different types of assemblies between the reward and
262 aversive conditions, we found that the joint assemblies were the most different between the two
263 valence conditions (**Figure 3C**). This suggests that synchronous neuronal activation spanning both
264 dHPC and vHPC provides finer contextual-emotional neural representations, potentially facilitating the
265 discrimination between two differentially valenced experiences.

266 Multiple studies already reported reactivations implicating the dHPC (G. Girardeau, Inema, and
267 Buzsáki 2017; Lansink et al. 2008; 2009; Pennartz et al. 2009) or vHPC (Miyawaki and Mizuseki
268 2022) in coordination with valence-related structures during sleep. Here we show that dorso-ventral
269 joint neuronal assemblies formed during an aversive exploratory behavior are selectively reactivated
270 during the following NREM sleep epoch. These reactivations do not occur for purely ventral or dorsal
271 assemblies following any of the two valence conditions. Why did only the joint aversive assemblies
272 show an increase in reactivation strength? One possible explanation is that, since the spatial
273 information between the two emotional run sessions is the same, the valence gains influence their
274 differentiation. Given the smaller overlap between condition representations in joint assemblies
275 compared to dorsal and ventral assemblies (**Figure 3A-B**), joint assemblies might be preferentially
276 reactivated to promote the discrimination between two differentially valenced experiences. Since the
277 vHPC has been mostly linked to the negative side of the valence spectrum (fear, anxiety, stress;
278 Ghasemi et al. 2022), the joint assemblies might be biased towards processing aversive-valenced
279 environments compared to reward-valenced environments during sleep.

280 The decay of reactivations along post-sleep time was not affected by the type of assemblies or
281 condition valence of the preceding exploration (**Figure 4B; Figure S10**). All assemblies tend to
282 reactivate during the first 20 minutes of post-sleep and then gradually decrease in activity.
283 Interestingly, this window of time for joint reactivations was previously reported in studies implicating

284 the vHPC (Miyawaki and Mizuseki 2022) and the dHPC (G. Girardeau, Inema, and Buzsáki 2017).
285 Reactivations in the dHPC and vHPC were shown to preferentially occur during respectively, dorsal
286 SWR and ventral SWR. Here, we found that joint dorsoventral aversive assemblies reactivate after
287 aversive experiences (**Figure 4**), and so selectively during dorsoventral coordinated SWRs (**Figure**
288 **5**).

289 In summary, we detected joint dorsoventral cell assemblies in the hippocampus that are reactivated
290 strongly during NREM sleep following aversive-motivated exploration, and to a lesser extent following
291 rewarded-motivated exploration. Compared to dorsal or ventral assemblies, joint assemblies showed
292 minor activity overlapping between the two emotional conditions suggesting that they might facilitate
293 the discrimination between two differentially-valenced environments. Joint assemblies reactivations
294 were stronger during dorsoventral coordinated SWRs after aversive and not after the reward
295 condition. Coordinated dorsoventral events are composed of bursts of SWRs and the proportion of
296 SWRs occurring in bursts increases particularly following aversive-condition. These findings suggest
297 that SWRs bursts and their dorsoventral coordination provide a physiological mechanism to integrate
298 context-emotion representations spanning dHPC and vHPC during sleep. We hypothesize that joint
299 reactivations of dHPC and vHPC during dorsoventral coordinated SWRs bursts are responsible for
300 sleep-dependent emotional processing. This is influenced by the preceding emotional valence, with a
301 stronger processing for aversive experiences than rewarded experiences. Further experiments are
302 required to deepen this hypothesis, such as using behavioral tasks that involve reward- or aversive-
303 driven learning to correlate dorsoventral sleep coordination with memory performance, or dynamically
304 perturbate this coordination to investigate its implication in emotional memory consolidation.

305

306 ## Contributions

307 FM and GG conceptualized the study, FM, EP and ILP performed the experiments, FM analyzed the
308 data. All authors contributed to writing the manuscript.

309

310 ## Funding

311 This work was funded by Fondation Fyssen, ATIP-Avenir, FSER (GG); EMBO (FM).

# Bibliography


Bannerman, D M, J. N.P. Rawlins, S. B. McHugh, R. M.J. Deacon, B K Yee, T Bast, W. N. Zhang, H. H.J. Pothuizen, and J Feldon. 2004. “Regional Dissociations within the Hippocampus - Memory and Anxiety.” *Neuroscience and Biobehavioral Reviews* 28 (3): 273–83. https://doi.org/10.1016/j.neubiorev.2004.03.004.

Binder, Sonja, Matthias Mölle, Michael Lippert, Ralf Bruder, Sonat Aksamaz, Frank Ohl, J. Simon Wiegert, and Lisa Marshall. 2019. “Monosynaptic Hippocampal-Prefrontal Projections Contribute to Spatial Memory Consolidation in Mice.” *Journal of Neuroscience* 39 (35): 6978–91. https://doi.org/10.1523/JNEUROSCI.2158-18.2019.

Buzsáki, György. 2015. “Hippocampal Sharp Wave-Ripple: A Cognitive Biomarker for Episodic Memory and Planning.” *Hippocampus* 25 (10): 1073–1188. https://doi.org/10.1002/hipo.22488.

Ciocchi, S, J Passecker, H Malagon-Vina, N Mikus, and T Klausberger. 2015. “Selective Information Routing by Ventral Hippocampal CA1 Projection Neurons.” *Science (New York, N.Y.)* 348 (6234): 560–63. https://doi.org/10.1126/science.aaa3245.

Davidson, T. J., F. Kloosterman, and M. A. Wilson. 2009. “Hippocampal Replay of Extended Experience.” *Neuron* 63 (4): 497–507.

Diba, Kamran, and György Buzsáki. 2007. “Forward and Reverse Hippocampal Place-Cell Sequences during Ripples.” *Nature Neuroscience* 10 (10): 1241–42. https://doi.org/10.1038/nn1961.

Dupret, David, Joseph O’Neill, Barty Pleydell-Bouverie, and Jozsef Csicsvari. 2010. “The Reorganization and Reactivation of Hippocampal Maps Predict Spatial Memory Performance.” *Nature Neuroscience* 13 (8): 995–1002. https://doi.org/10.1038/nn.2599.

Ego-Stengel, Valérie, and Matthew A. Wilson. 2009. “Disruption of Ripple-Associated Hippocampal Activity during Rest Impairs Spatial Learning in the Rat.” *Hippocampus*, NA-NA. https://doi.org/10.1002/hipo.20707.

Fanselow, Michael S, and Hong-Wei Dong. 2010. “Are the Dorsal and Ventral Hippocampus Functionally Distinct Structures?” *Neuron* 65 (1): 7–19. https://doi.org/10.1016/j.neuron.2009.11.031.

Forro, Thomas, Emmanouela Volitaki, Hugo Malagon-Vina, Thomas Klausberger, Thomas Nevian, and Stéphane Ciocchi. 2022. “Anxiety-Related Activity of Ventral Hippocampal Interneurons.” *Progress in Neurobiology* 219 (December):102368. https://doi.org/10.1016/j.pneurobio.2022.102368.

Foster, David J, and Matthew a Wilson. 2006. “Reverse Replay of Behavioural Sequences in Hippocampal Place Cells during the Awake State.” *Nature* 440 (7084): 680–83. https://doi.org/10.1038/nature04587.

Ghasemi, Maedeh, Mojdeh Navidhamidi, Fatemeh Rezaei, Armin Azizikia, and Nasrin Mehranfard. 2022. “Anxiety and Hippocampal Neuronal Activity: Relationship and Potential Mechanisms.” *Cognitive, Affective, & Behavioral Neuroscience* 22 (3): 431–49. https://doi.org/10.3758/s13415-021-00973-y.

Girardeau, G., I. Inema, and G. Buzsáki. 2017. “Reactivations of Emotional Memory in the Hippocampus-Amygdala System during Sleep.” *Nature Neuroscience* 20 (11). https://doi.org/10.1038/nn.4637.

Girardeau, Gabrielle, Karim Benchenane, Sidney I Wiener, György Buzsáki, and Michaël B Zugaro. 2009. “Selective Suppression of Hippocampal Ripples Impairs Spatial Memory.” *Nature Neuroscience* 12 (10): 1222–23. https://doi.org/10.1038/nn.2384.

Harvey, Ryan E., Heath L. Robinson, Can Liu, Azahara Oliva, and Antonio Fernandez-Ruiz. 2023. “Hippocampo-Cortical Circuits for Selective Memory Encoding, Routing, and Replay.” *Neuron* 111 (13): 2076-2090.e9. https://doi.org/10.1016/j.neuron.2023.04.015.

Herbst, Matthew R., Robert C. Twining, and Marieke R. Gilmartin. 2022. “Ventral Hippocampal Shock Encoding Modulates the Expression of Trace Cued Fear.” *Neurobiology of Learning and Memory*

190 (April):107610. https://doi.org/10.1016/j.nlm.2022.107610.

Hollup, S. A., S. Molden, J. G. Donnett, M. B. Moser, and E. I. Moser. 2001. “Accumulation of Hippocampal Place Fields at the Goal Location in an Annular Watermaze Task.” *The Journal of Neuroscience* 21 (5): 1635–44.

Huff, Mary L, Eric B Emmons, Nandakumar S Narayanan, and Ryan T LaLumiere. 2016. “Basolateral Amygdala Projections to Ventral Hippocampus Modulate the Consolidation of Footshock, but Not Contextual, Learning in Rats.” *Learning and Memory* 23 (2): 51–60. https://doi.org/10.1101/lm.039909.115.

Jimenez, Jessica C., Jack E. Berry, Sean C. Lim, Samantha K. Ong, Mazen A. Kheirbek, and Rene Hen. 2020. “Contextual Fear Memory Retrieval by Correlated Ensembles of Ventral CA1 Neurons.” *Nature Communications* 11 (1): 3492. https://doi.org/10.1038/s41467-020-17270-w.

Jimenez, Jessica C., Katy Su, Alexander R. Goldberg, Victor M. Luna, Jeremy S. Biane, Gokhan Ordek, Pengcheng Zhou, et al. 2018. “Anxiety Cells in a Hippocampal-Hypothalamic Circuit.” *Neuron* 97 (3): 670-683.e6. https://doi.org/10.1016/j.neuron.2018.01.016.

Jung, Min W, S I Wiener, and B L McNaughton. 1994. “Comparison of Spatial Firing Characteristics of Units in Dorsal and Ventral Hippocampus of the Rat.” *The Journal of Neuroscience* 14 (12): 7347–56.

Kjelstrup, Kirsten Brun, Trygve Solstad, Vegard Heimly Brun, Torkel Hafting, Stefan Leutgeb, Menno P. Witter, Edvard I. Moser, and May-Britt Moser. 2008. “Finite Scale of Spatial Representation in the Hippocampus.” *Science* 321 (5885): 140–43. https://doi.org/10.1126/science.1157086.

Lansink, Carien S, Pieter M Goltstein, Jan V Lankelma, Ruud N J M a Joosten, Bruce L McNaughton, and Cyriel M a Pennartz. 2008. “Preferential Reactivation of Motivationally Relevant Information in the Ventral Striatum.” *The Journal of Neuroscience : The Official Journal of the Society for Neuroscience* 28 (25): 6372–82. https://doi.org/10.1523/JNEUROSCI.1054-08.2008.

Lansink, Carien S, Pieter M Goltstein, Jan V Lankelma, Bruce L Mcnaughton, and Cyriel M A Pennartz. 2009. “Hippocampus Leads Ventral Striatum in Replay of Place-Reward Information.” *PLoS Biology* 7 (8): e1000173. https://doi.org/10.1371/journal.pbio.1000173.

Lopes-dos-Santos, Vítor, Sidarta Ribeiro, and Adriano B L Tort. 2013. “Detecting Cell Assemblies in Large Neuronal Populations.” *Journal of Neuroscience Methods* 220 (2): 149–66. https://doi.org/10.1016/j.jneumeth.2013.04.010.

Malik, Ruchi, Yi Li, Selin Schamiloglu, and Vikaas S. Sohal. 2022. “Top-down Control of Hippocampal Signal-to-Noise by Prefrontal Long-Range Inhibition.” *Cell* 185 (9): 1602-1617.e17. https://doi.org/10.1016/j.cell.2022.04.001.

Miyawaki, Hiroyuki, and Kenji Mizuseki. 2022. “De Novo Inter-Regional Coactivations of Preconfigured Local Ensembles Support Memory.” *Nature Communications* 13 (1): 1272. https://doi.org/10.1038/s41467-022-28929-x.

Moita, Marta a P, Svetlana Rosis, Yu Zhou, Joseph E LeDoux, and Hugh T Blair. 2004. “Putting Fear in Its Place: Remapping of Hippocampal Place Cells during Fear Conditioning.” *The Journal of Neuroscience : The Official Journal of the Society for Neuroscience* 24 (31): 7015–23. https://doi.org/10.1523/JNEUROSCI.5492-03.2004.

O’Keefe, John. 1976. “Place Units in the Hippocampus of the Freely Moving Rat.” *Experimental Neurology* 51 (1): 78–109. https://doi.org/10.1016/0014-4886(76)90055-8.

O’Neill, Joseph, Barty Pleydell-Bouverie, David Dupret, and Jozsef Csicsvari. 2010. “Play It Again: Reactivation of Waking Experience and Memory.” *Trends in Neurosciences* 33 (5): 220–29. https://doi.org/10.1016/j.tins.2010.01.006.

Patel, Jagdish, Erik W Schomburg, A Berenyi, Shigeyoshi Fujisawa, György Buzsáki, and Antal Berényi. 2013. “Local Generation and Propagation of Ripples along the Septotemporal Axis of the Hippocampus.” *J Neurosci* 33 (43): 17029–41. https://doi.org/33/43/17029 [pii]\n10.1523/JNEUROSCI.2036-13.2013.

Pennartz, Cyriel M a, Joshua D Berke, Ann M Graybiel, Rutsuko Ito, Carien S Lansink, Matthijs van

der Meer, a David Redish, Kyle S Smith, and Pieter Voorn. 2009. “Corticostriatal Interactions during Learning, Memory Processing, and Decision Making.” *The Journal of Neuroscience : The Official Journal of the Society for Neuroscience* 29 (41): 12831–38. https://doi.org/10.1523/JNEUROSCI.3177-09.2009.

Pitkänen, Asla, Maria Pikkarainen, Nina Nurminen, and Aarne Ylinen. 2000. “Reciprocal Connections between the Amygdala and the Hippocampal Formation, Perirhinal Cortex, and Postrhinal Cortex in Rat: A Review.” *Annals of the New York Academy of Sciences* 911 (1): 369–91. https://doi.org/10.1111/j.1749-6632.2000.tb06738.x.

Pompili, Marco N., Noé Hamou, and Sidney I. Wiener. 2024. “Differential Encoding of Fear Learning and Fear Expression in the Ventral and Dorsal Hippocampus.” Preprint. Neuroscience. https://doi.org/10.1101/2024.01.26.577384.

Pronier, Éléonore. n.d. “The Role of the Hippocampus in the Consolidation of Emotional Memories during Sleep.” *Trends in Neurosciences*.

Schuette, Peter J., Fernando M. C. V. Reis, Sandra Maesta-Pereira, Meghmik Chakerian, Anita Torossian, Garrett J. Blair, Weisheng Wang, et al. 2020. “Long-Term Characterization of Hippocampal Remapping during Contextual Fear Acquisition and Extinction.” *The Journal of Neuroscience* 40 (43): 8329–42. https://doi.org/10.1523/JNEUROSCI.1022-20.2020.

Skaggs, W E, and B L McNaughton. 1996. “Replay of Neuronal Firing Sequences in Rat Hippocampus during Sleep Following Spatial Experience.” *Science (New York, N.Y.)* 271 (5257): 1870–73.

Strange, Bryan a., Menno P. Witter, Ed S. Lein, and Edvard I. Moser. 2014. “Functional Organization of the Hippocampal Longitudinal Axis.” *Nature Reviews Neuroscience* 15 (10): 655–69. https://doi.org/10.1038/nrn3785.

Ven, Gido M van de, Stéphanie Trouche, Colin G. G McNamara, Kevin Allen, David Dupret, Gido M. van de Ven, Stéphanie Trouche, Colin G. G McNamara, Kevin Allen, and David Dupret. 2016. “Hippocampal Offline Reactivation Consolidates Recently Formed Cell Assembly Patterns during Sharp Wave-Ripples.” *Neuron*, 1–7. https://doi.org/10.1016/j.neuron.2016.10.020.

Wang, Dong V, Hau-jie Yau, Carl J Broker, Jen-hui Tsou, Antonello Bonci, and Satoshi Ikemoto. 2015. “Mesopontine Median Raphe Regulates Hippocampal Ripple Oscillation and Memory Consolidation.” *Nature Neuroscience* 18 (April). https://doi.org/10.1038/nn.3998.

Wang, Gong-Wu, Jian Liu, and Xiao-Qin Wang. 2017. “Post-Training Reversible Disconnection of the Ventral Hippocampal–Basolateral Amygdaloid Circuits Impairs Consolidation of Inhibitory Avoidance Memory in Rats.” *Learning & Memory* 24 (11): 602–6. https://doi.org/10.1101/lm.044701.116.

Wilson, M a, and B L McNaughton. 1993. “Dynamics of the Hippocampal Ensemble Code for Space.” *Science (New York, N.Y.)* 261 (5124): 1055–58.

Wilson, Matthew A, and Bruce L McNaughton. 1994. “Reactivation of Hippocampal Ensemble Memories During Sleep.” *Science* 265 (14): 676–79.

449 ## Material and Methods

450 **Ethical Statement**. All experimental procedures were performed following the official European
451 guidelines for the care and use of laboratory animals (86/609/EEC), the Policies of the French
452 Committee of Ethics (Decrees n° 87-848 and n° 2001–464), and after approval by ethical committee
453 (APAFIS #35991-2022031810445522 v3).

454

455 **Subjects and electrode implantation**. This project included six individually housed female Long-
456 Evans (Rats id: 103, 126, 127, 128, 132, 165) and maintained on a 12h:12h light-dark cycle during
457 experiments. For the surgery animals (300g 3 months old at the time of the surgery) were injected
458 with buprenorphine (Vetergesic® - 0.3mg/ml, dose: 0.05mg/kg) before anesthesia induction. For the
459 whole surgery time animals were deeply anesthetized with isoflurane. Following the loss of reflex we
460 subcutaneously injected the local anesthetic Lidocaine (Lidor®- 20mg/mL, dose: 4mg/kg)on the scalp,
461 after 15 minutes of the Lidocaíne injection an incision was performed to open access to the skull.
462 Corporal temperature was monitored throughout the surgery and maintained at 37°C using a heating
463 pad. Small metal screws were placed at different points in the skull as anchors for the implant. Two or
464 three electrodes mounted on individual movable nano-drives (Cambridge nano-drives,
465 size(2x5x11mm)) were implanted above the vHPC unilaterally (initial position, AP: -5.50mm, LAT:
466 4.10mm, DV: -6.5mm, angle: 10°) and in the dHPC either unilaterally or bilaterally (initial position, AP:
467 -3.50mm, LAT: 2.50mm, DV: -1.7mm). Dental cement was used to anchor the microdrives. To target
468 the vHPC we used an 8-shank silicon probe (NeuroNexus Buzsaki64L), while for the dHPC we used
469 either a 4-shank silicon probe (NeuroNexus Buzsaki32) or a customized array constituted of 8
470 tetrodes (20 µm insulated tungsten wire) arranged in a straight line. Two screws located on the
471 occipital bone were used as ground and reference. The drives and probes were protected by a
472 cement-covered copper-mesh Faraday cage on which the probe connectors were attached. We
473 implanted a bipolar electrode in the eyelid to administer electric shocks during aversive runs. This
474 involved introducing two 140 µm silver wires between the skin and the muscle surrounding the eyelid.
475 The external tips of the wires were then soldered to connectors fixed to the copper mesh. During the
476 two first days following the surgery, animals were injected with a combination of Buprenorphine
477 (Vetergesic® - 0.3mg/ml, dose: 0.05mg/kg), and Meloxicam (Metacam®- 5mg/mL, dose: 1mg/kg).

Animals were allowed to recover for at least 5 days with ad libitum food and water. In Rat 126, the dHPC probe failed reaching to the pyramidal layer during the experiment. Thus, only vHPC data was used from this animal.

**Recordings and Behavior**. All animals were free from prior manipulation before being included in the study. After at least 5 days of daily handling, animals were water-deprived and trained to run back and forth on a linear track for water rewards. All experiments were performed during the light cycle. After 7 days of training, animals regained access to ad libitum water and were exposed to the electrode implantation surgery 3 days later. After the recovery period, animals were water-deprived again and re-exposed to the rewarded linear track task for at least 2 days. Subsequently, animals were exposed to three daily training sessions composed of a rewarded and an aversive-motivated linear track exploration. Before and after each run condition, animals were allowed to sleep for at least 2 hours. During aversive run sessions, animals were provided water at the end of each lap for a specific period, while the remainder of the time, they received an electric shock to the eyelid if they remained motionless for at least 20 seconds. The reward time was progressively reduced during aversive runs across training days until only shocks were delivered if the animal remained quiet. Task sessions were composed of pure reward and pure aversive run sessions, preceded and followed by sleep sessions (Figure 1A-B). At the end of each recording day, animals were reintroduced to ad libitum water for 5 to 20 minutes to ensure the animals remained>80% of their normal weight. The probes were slowly lowered in the brain to reach dorsal and ventral pyramidal layers after finishing the training sessions. Probes were adjusted daily to optimize ripple and unit recording. We tried to maximize the chances of getting usable data once the animal reached a plateau performance in the aversive condition. Signals were recorded at 20 kHz using an Intan recording system (Intan Technologies, California, United States of America). The videos, captured at 30 fps with a Basler camera (ace Basler 106754), were synchronized with the Intan system via the digital input for retrospective matching of animal behavior with electrophysiological data. Instantaneous speed was calculated using the neck position extracted from the videos using DeepLab Cut (DeepLabCut2.0 Toolbox, Mathis, A., et. all 2018).

**Preprocessing**. Electrophysiological data was sampled at 20 kHz and resampled at 1250Hz to extract LFP data. Spikes were extracted by high-pass filtering and thresholding the signal, then clustered using Kilosort 2.5 (Steinmetz, et. al. 2019b) followed by manual curation using Phy (Rossant et al., 2016). Sleep stages were manually scored through visual inspection of the dorsal and ventral hippocampal spectrograms and accelerometer signals using TheStateEditor, a custom program from the FMA toolbox (http://fmatoolbox.sourceforge.net/). We defined NREM epochs as periods characterized by immobility and low theta/delta ratio, while REM sleep was characterized by immobility and regular theta waves (Figure S5). Ripple detection was performed by band-pass filtering (~100–200 Hz), squaring and z-scoring, and thresholding the field potential recorded in the dorsal and ventral CA1 pyramidal layer. SWRs were defined as events starting at 2 or 3 standard deviations (s.d.) and peaking at greater than 5 or 7 s.d. for dorsal or ventral SWRs, respectively. Ripple events in both regions could last less than 100 ms and more than 20 ms around the peak.

**Statistical analysis**. Statistical analyses were performed using Matlab R2020a. For comparisons between the two groups, we used a two-tailed unpaired Wilcoxon rank-sum test. When analyzing more than two groups, we used the Kruskal-Wallis test for unpaired data and the Friedman test for paired, followed by the Tukey-Kramer post-hoc test. If the data met the criteria for normality, we used Student's t-tests for two-group comparisons and one-way ANOVA followed by the Tukey-Kramer post-hoc test for multiple-group comparisons. Data presented in cumulative graphs were compared using the Kolmogorov-Smirnov test. Correlations between continuous variables were examined by linear regression. A significance level of $p<0.05$ was considered statistically significant unless otherwise stated. The specific tests used for each analysis are described in the figure legends or the text. Data distribution was visualized using scatter plots, with the mean plotted or box plots showing the median and quintiles.

**Analysis**. All analyses were performed using customized toolboxes (Chronux, FMA toolbox), built-in functions, and custom-written scripts in Matlab (The MathWorks, Inc., Natick, MA, USA).

535 **Dorsal-ventral ripples coordination**. First, We constructed a peri-event histogram of ventral SWR
536 peaks locked to dorsal ones using the ccg function from FMAtoolbox and normalized it to the total
537 amount of ventral SWRs (10-msec bins). By visually inspecting the CCG, we defined coordinated
538 events to those dorsal-ventral ripple pairs occurring +/-100ms from each other. To ascertain whether
539 the percentage of coordinated dorsal and ventral ripples exceeded the chance level, we shuffled the
540 referenced ripple peaks 100 times and calculated the percentage of coordinated reference ripples.
541 This process yielded a surrogate average percentage value compared with the value obtained in each
542 session. For autocorrelograms and crosscorrelograms in Figure 4, we used 10-msec bins.

543

544 **Ripple bursts analyses**. We defined a ripple burst to all subsequent ripple peaks with <100ms
545 between each other. The beginning and end of each burst were determined as the beginning of the
546 first ripple and the end of the last one from the burst. To construct the cross-correlograms between
547 dorsal and ventral ripple bursts, we also calculated the central time point of each event.

548

549 **Single-units analyses**. We detected 1071 single units in the dHPC and 544in the vHPC. Units were
550 classified into putative pyramidal cells and putative interneurons based on waveform shape as
551 described previously (Bartho et al.,2004; Figure S3). Briefly, duration at 50% from baseline to peak
552 (distance A) and peak-to-trough time (distance B) were utilized for clustering with k-means into 2
553 clusters, interneurons, and pyramidal cells. The gain firing rate locked to ripple peaks was calculated
554 in 10-msec bin by dividing the firing rate in each bin by the baseline firing rate outside SPW-Rs (inter-
555 ripple NREM intervals). To define if a unit was ripple-modulated, we performed a Poisson test with $P <$
556 $0.001$.

557

558 **Assembly patterns detection**. To do so, we constructed a spike train of each putative-pyr single unit
559 using 25-ms, pooling dorsal and ventral units. Time bin was defined as it was proposed that at this
560 time scale detection of assembly, expression is optimal (Harris et al., 2003; van de ven et al 2016),
561 and after corroborating that different time bins (5, 10, 25, 50, 100 ms, data not shown) were not
562 drastically increasing the ratio made by the number of detected assemblies over the number of

significantly similar patterns. To avoid a bias due to a higher firing rate, spike trains were z-scored. Assembly patterns were identified using a two-step process (Figure S6) described by Lopes-dos-Santos et al, 2013. Briefly, the first step was determining the number of significant co-activation patterns present in each recording session. To do so, the algorithm counted the principal component variances that exceeded a threshold determined by an analytical probability function for uncorrelated data (Marčenko-Pastur distribution). Secondly, independent component analysis (ICA) was employed to extract the assembly patterns from the data projection within the subspace defined by initially detected significant principal components. As templates, we used mobility periods (>7 cm/sec during more than 2 seconds) in the Aversive or the Rewarded run sessions. After detecting the assembly patterns, those units whose weights exceeded the threshold defined as abs($1/\sqrt{N}$)were defined as assembly members. If members were coming from the dorsal or ventral hippocampal units, the assemblies were defined as dHPC or vHPC respectively. If they were coming from both regions, we named those as joint assemblies.

To track assembly pattern expression over time (Figure S6), a projection matrix was created for each pattern using its weight vector's outer product, with the main diagonal set to zero. To maximize the role of members in assembly activations, we set to zero the weight of non-member units. Each neuron's spike train was convolved with a Gaussian kernel and z-scored for high temporal resolution. The expression strength of a pattern at any time was defined by the quadratic form of its projection matrix with the smoothed and z-scored firing rate vector. Peaks in expression strength above 5 were identified and used for subsequent analyses. For reactivation rate calculation, we counted the reactivation peaks in 60-second bins during Pre- and Post-sleep. To minimize the overlap between the Post-sleep of the first emotional condition and the Pre-sleep of the second one, we restricted NREM or REM epochs to those occurring 1 hour before or after each run session. For Peak Reactivation Strength calculation, we averaged the reactivation values of peaks occurring during Post-sleep and subtracted the average of the peak values in Pre-sleep. Finally, we divided by the average value of all peaks detected during both sleep sessions. Note that if this metric is positive and significantly different from zero, it means that the average reactivation peak values were higher in the Post-sleep period. We also measured the Reactivation Strength during coordinated and uncoordinated dorsal-ventral ripples.

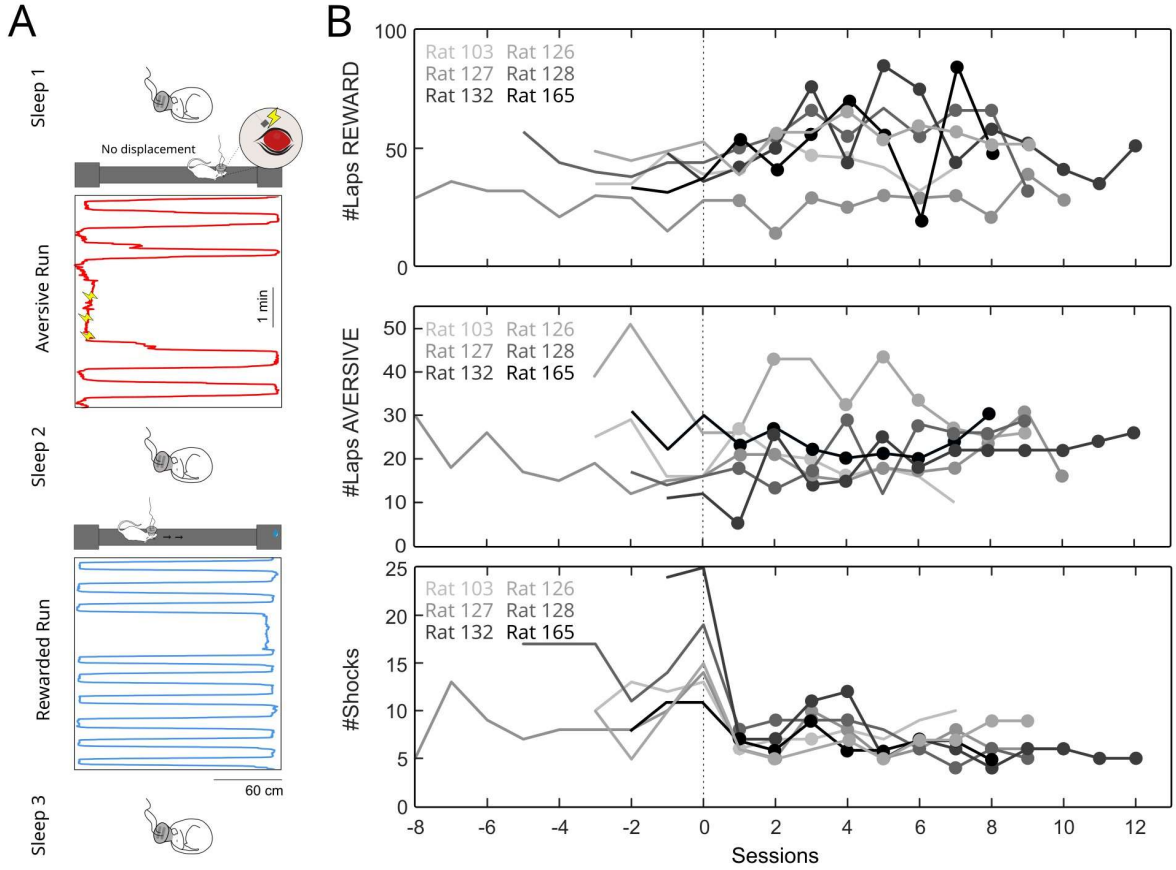


**Figure 1: Rats alternate between aversive and rewarded motivated exploration of a linear track**. (A) Rats run back and forth on a linear track to avoid eye-lid shocks (Aversive Run) or receive a water drop (Reward Run). Before and after each run session, animals are allowed to sleep in their home cage. (B) Animals showed a reduced number of shocks received in aversive run sessions, without alternating the number of reward laps made in the rewarded run sessions. $N_{sessions}$=47.

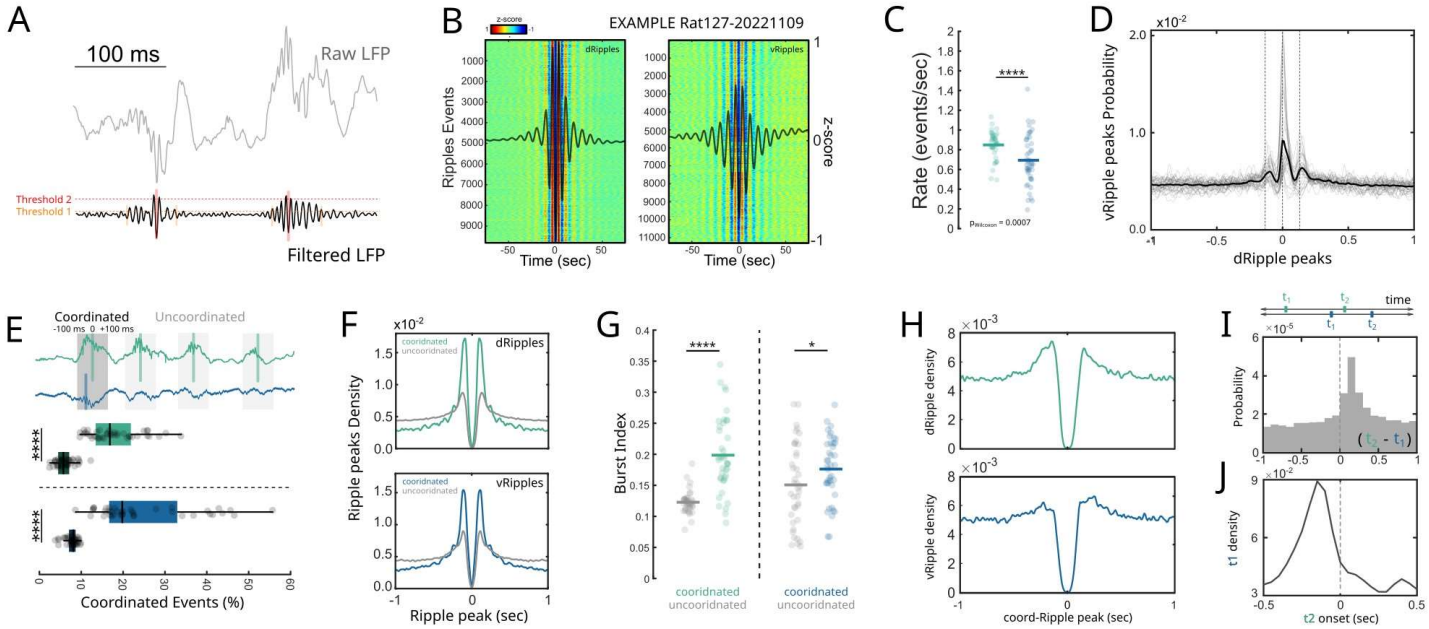


**Figure 2: Ripples coordination across dorsal-ventral hippocampal axis**. (A) Ripples in both regions were detected by thresholding the normalized squared local-field potential signal filtered between 100Hz and 250Hz. (B) Colormap showing z-scored signal surrounding the peak of each detected dorsal (left) and ventral ripple (right). (C) Ripple rate calculated during NREM sleep in the dorsal (green) and ventral (blue) hippocampus. Wilcoxon rank sum test, ****p=0,0007, $N_{dHPC}$=40, $N_{vHPC}$=47. (D) Peristimulus histogram showing the ventral ripple peaks density surrounding dorsal ripple peaks. Each gray line is a session, and the average across them is represented in black. Note the existence of three peaks in this graph in +/- 100ms (marked with dashed lines). (E) Coordinated events were defined as a pair of dorsal-ventral ripples that occurred with a delay of less than 100 ms. We found that the percentage of coordinated events was different from the chance level. Wilcoxon rank sum test, ****p<0.0001, N=40. (F) Average autocorrelogram of ripple peaks timestamps from coordinated and uncoordinated (in gray). (G) Burst Index of coordinated and uncoordinated ripples from the dorsal and ventral hippocampus. Wilcoxon rank sum test, *p<0.05, ****p<0.0001, N=40. (H) Average cross-correlogram between coordinated and uncoordinated ripple peaks from dorsal (upper panel) and ventral hippocampus (lower panel). (I) Histogram of the time difference between the end of dorsal ripple bursts and the beginning of ventral ones. (J) Crosscorrelogram of the beginning of the ventral bursts locked to the end of the dorsal ones.

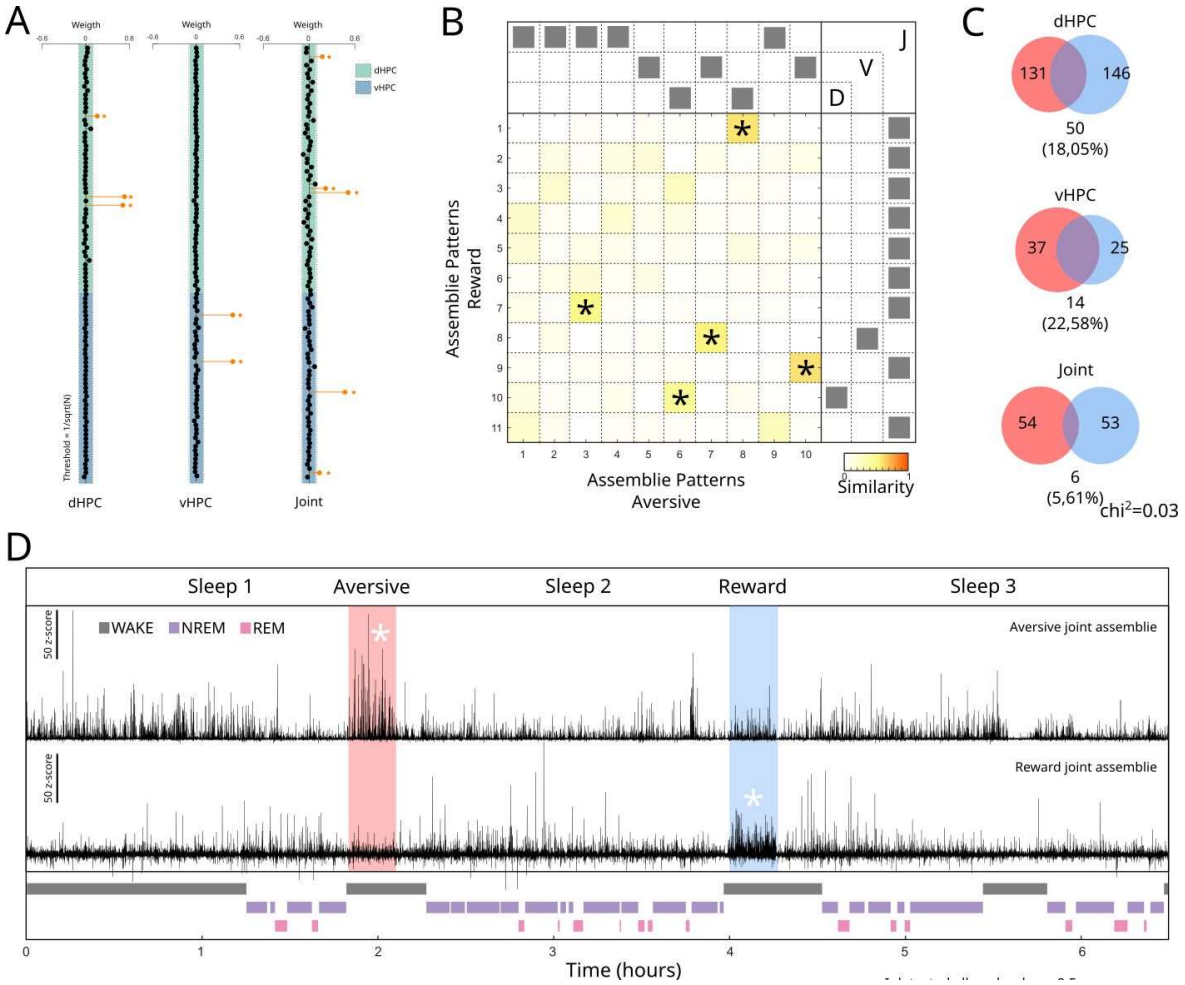


**Figure 3: Assemblies detection during Aversive and Rewarded runs**. We detected assemblies using the spike trains of dorsal and ventral putative-pyramidal hippocampal units. (A) Three examples of assemblies that exceeded the MarcenkoPastur threshold from a representative session (Rat128, session4). We defined a unit as an assemblies members (orange lollipops) when its ICA weight exceed a threshold (abs(1/√N)). Assemblies were tagged depending on the structure which members were coming from (dHPC, vHPC, or joint). (B) Example of an Assembly Similarity Index matrix. This index was calculated as the dot product of different assembly pairs. A pair of assemblies was considered significantly similar if the Similarity index was above the 99.9 percentile of a surrogate distribution (marked with * in the example). (C) Venn diagrams representing the proportions of assemblies detected in aversive (in red) and reward runs (in blue). The overlapping area between both circles represents the proportion of assemblies that were significantly similar between conditions. Note that joint assemblies showed lower overlapping between conditions in comparison to dHPC and vHPC assemblies. $Chi^2$, p=0,03. (D) Examples of assembly activity trace from a joint aversive (upper) and a joint rewarded assemblies (lower).

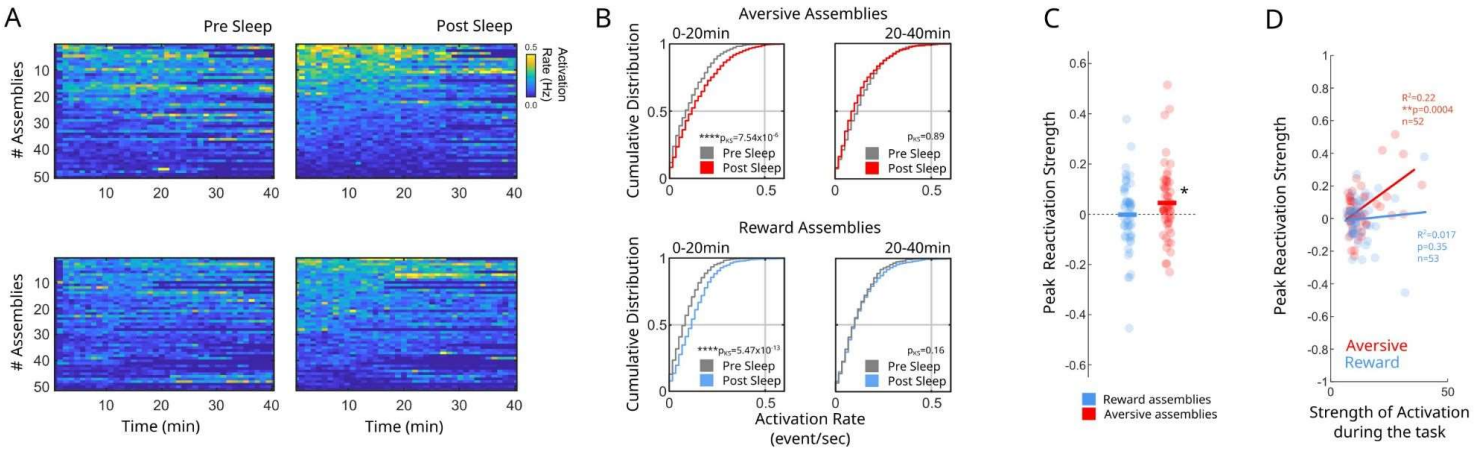


**Figure 4: Joint assemblies reactivation during NREM sleep.** (A) Assemblies activation rate across time during pre- and post-sleep sessions. We detected the peaks from aversive (upper) and rewarded (lower) assemblies' activity and calculated the rate in 60-second bins. (B) Cumulative graphs including pre- (in gray) and aversive or rewarded post-sleep reactivation rates (in red or blue, respectively). Note that there is a significant increase in activation rate in the post against pre-sleep in both types of assemblies that diminished over the sleep session. Kolmogórov-Smirnov test, ****p<0,0001. (C) Peak Reactivation Strength from aversive and reward assemblies. It was calculated as the average of the peak value from the post-sleep minus those coming from the pre-sleep divided by the peak value average from both sleep sessions. Note that only joint-aversive assemblies showed a significant increase compared to zero. Wilcoxon test, *p=0,014. (D) Joint aversive assemblies' Reactivation strength correlates with their activation during the task. Linear regression, **p<0.001. $N_{aversive}$= 54, $N_{reward}$=53.

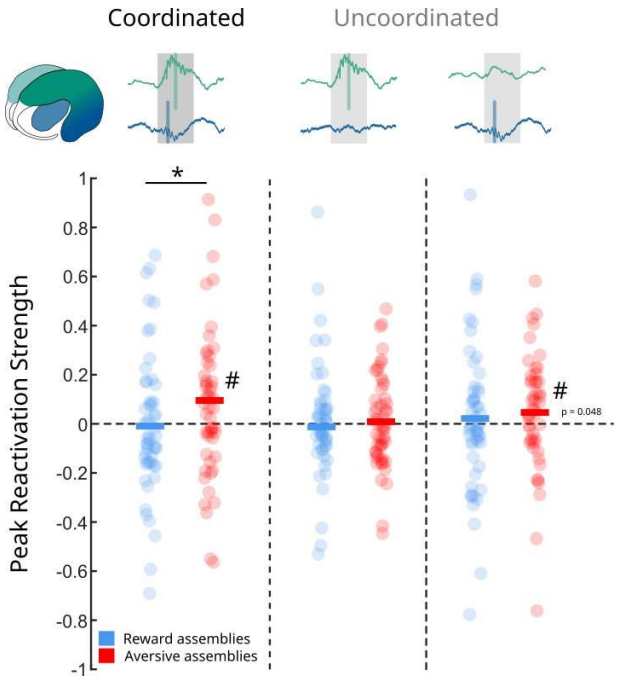


**Figure 5: Joint aversive assemblies increase their reactivation strength selectively during dorsal-ventral coordinated ripples**. Average peak reactivation strength was calculated for joint aversive and reward assemblies during dorsal-ventral coordinated ripples and dorsal or ventral ripples occurring uncoordinatedly. Only joint-aversive assemblies showed a significant increase against zero. Wilcoxon signed rank, $^{\#}p=0.033$. Also, they showed a significant increase compared to joint-reward assemblies' reactivation strength. Wilcoxon signed rank, $^{*}p=0.032$, $N_{aversive}=54$, $N_{reward}=53$.

Supplementary Figures

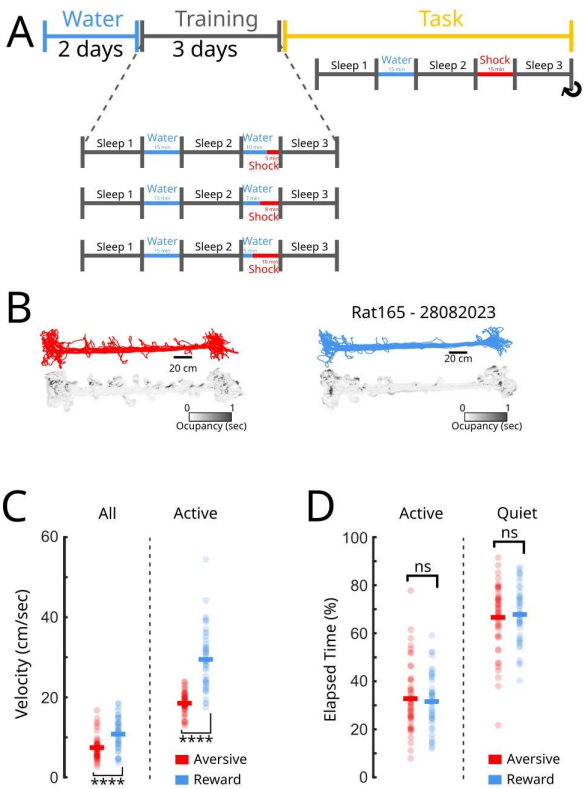


**Supplementary Figure 1: Distribution of speed, quiet, and active periods across the linear track**. (A) After probe implantation, animals were re-trained to perform in the reward running. During training sessions, we trained animals for the aversive run by giving them water during that session and progressively extracting it. (B) Examples of aversive (left) and rewarded-motivated exploration (right). Active periods were defined as moments where the animals showed an instantaneous speed of >7m/sec for at least 2 seconds. (C) Average velocity for aversive and rewarded-run sessions pooling all the time or just keeping the active periods. (D) Elapsed time the animals showed during active and quiet periods.

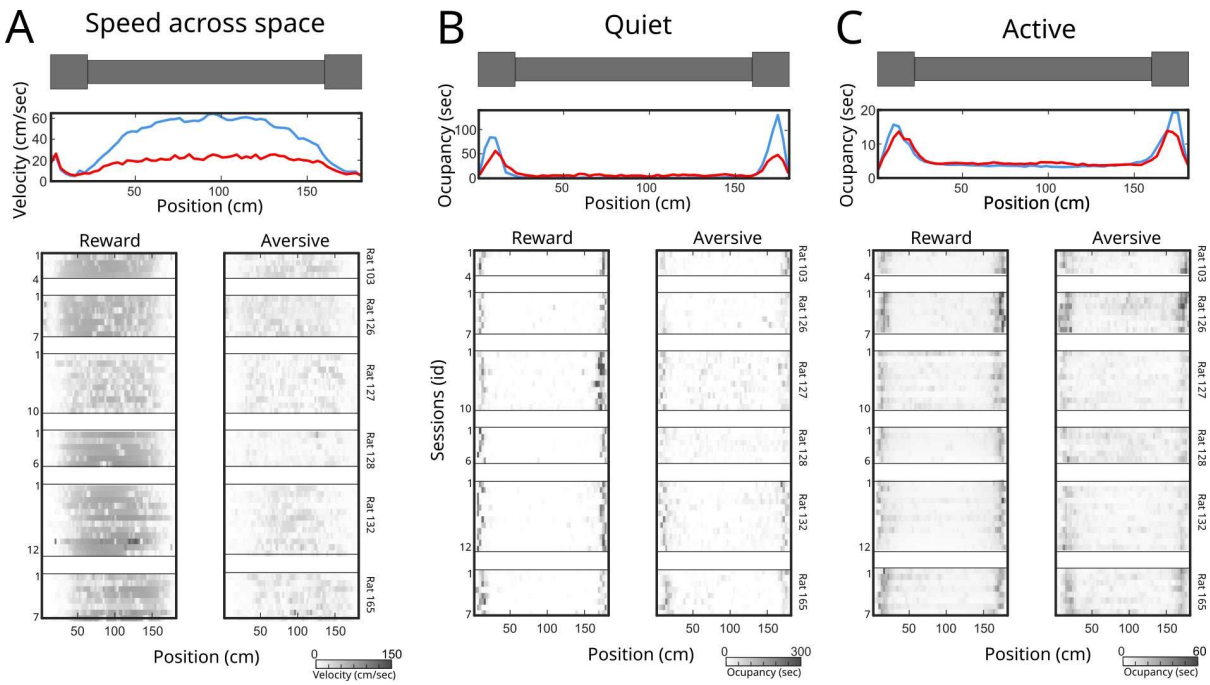


**Supplementary Figure 2: Distribution of speed, quiet, and active periods across the linear track**. The upper panels present an average across aversive (in red) and reward (in blue) sessions. Colormaps of each variable for aversive (right) and reward (left) are presented in the lower panels. In these graphs, each line contains the average data for each session. (A) Speed distribution across different positions in the linear track. In the upper panels, the average for each plotted variable. Quiet periods were defined as the moments when the animal was not active. Occupancy across the space being (B) quiet or (C) active. N=47.

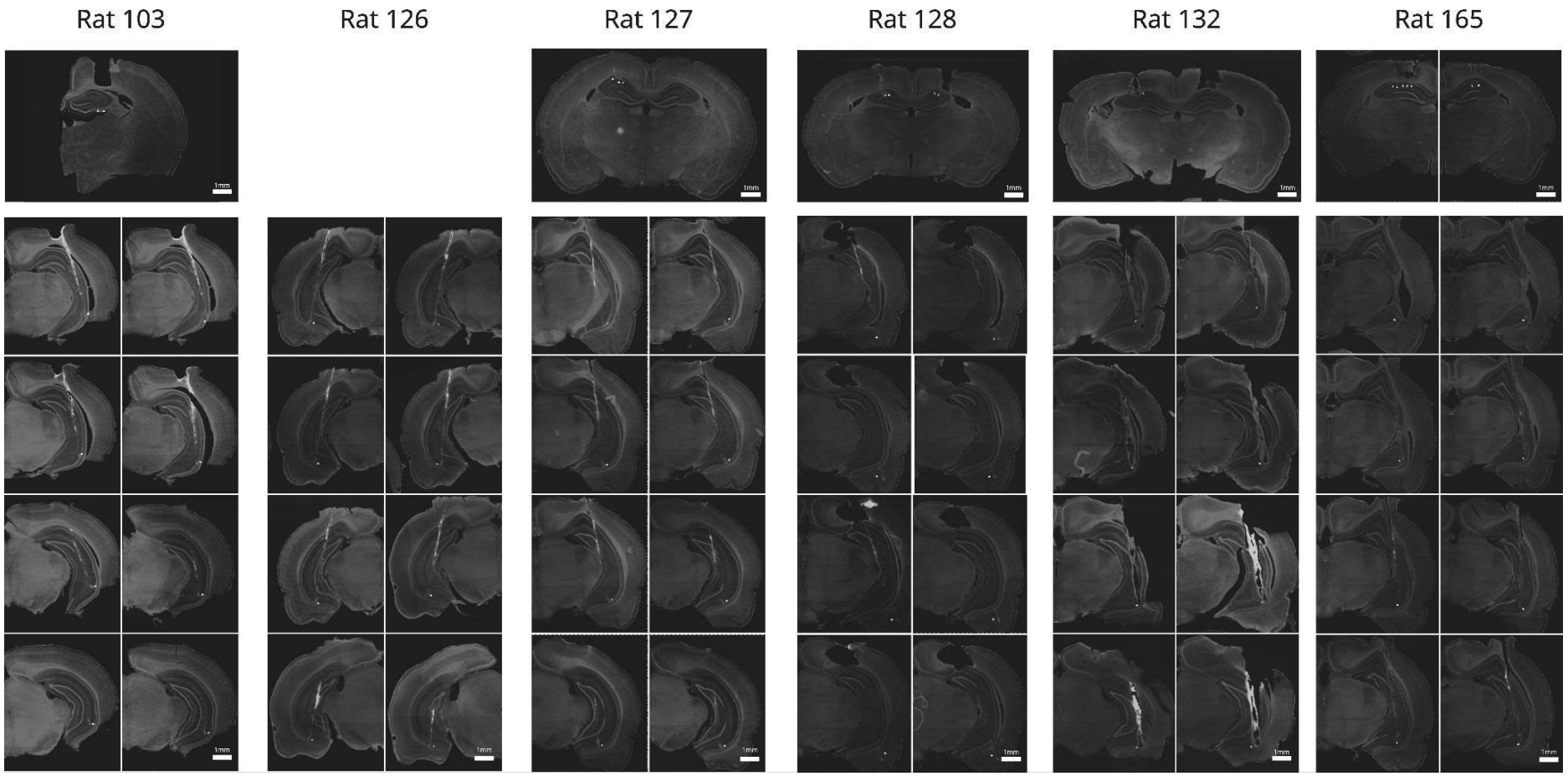


**Supplementary Figure 3: Histological reconstruction of electrode placement in dorsal and ventral hippocampus**. After histological reconstruction, we corroborated that in five rats (Rats 103, 127, 127, 132, 165), we reached both the dorsal and ventral pyramidal layers, while in Rat 126, we acquired good data only from the ventral hippocampus.

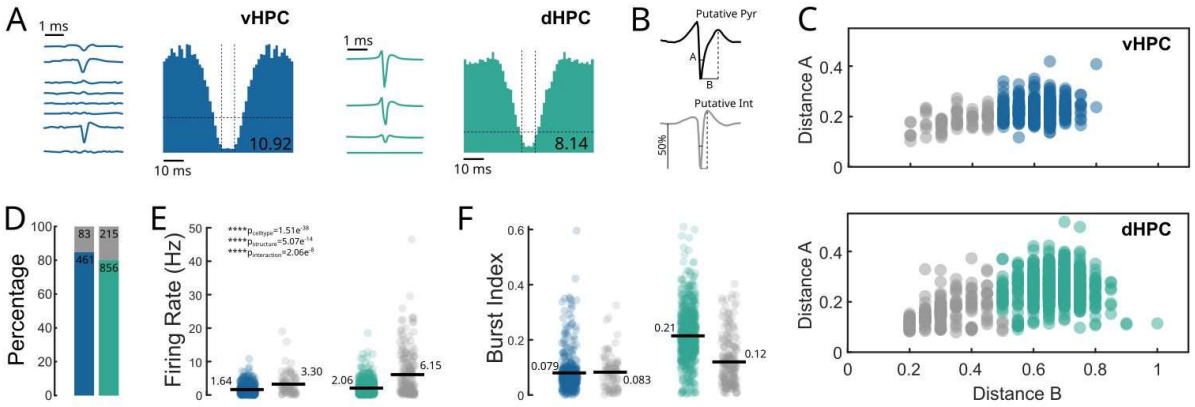


**Supplementary Figure 4: Single-units waveform classification**. Single units were manually curated using their autocorrelogram and waveform. (A) Examples of ventral (left panel, in blue) and dorsal (right panel, in green) single units. (B) They were classified between putative pyramidal cells (Pyr) or putative interneurons (Int) using duration at 50% from baseline to peak (distance A) and peak-to-trough time (distance B). (C) The clustering was performed with k-means with 2 clusters on the waveform properties of the cells (interneurons in gray and pyramidal cells in blue or green). (D) The majority of units from both regions were classified as putative pyramidal cells. (E) The firing rate was higher in putative interneurons compared to putative pyramidal cells in both regions. (F) Consistently with the literature, putative pyramidal cells in the dHPC showed a higher burst index.

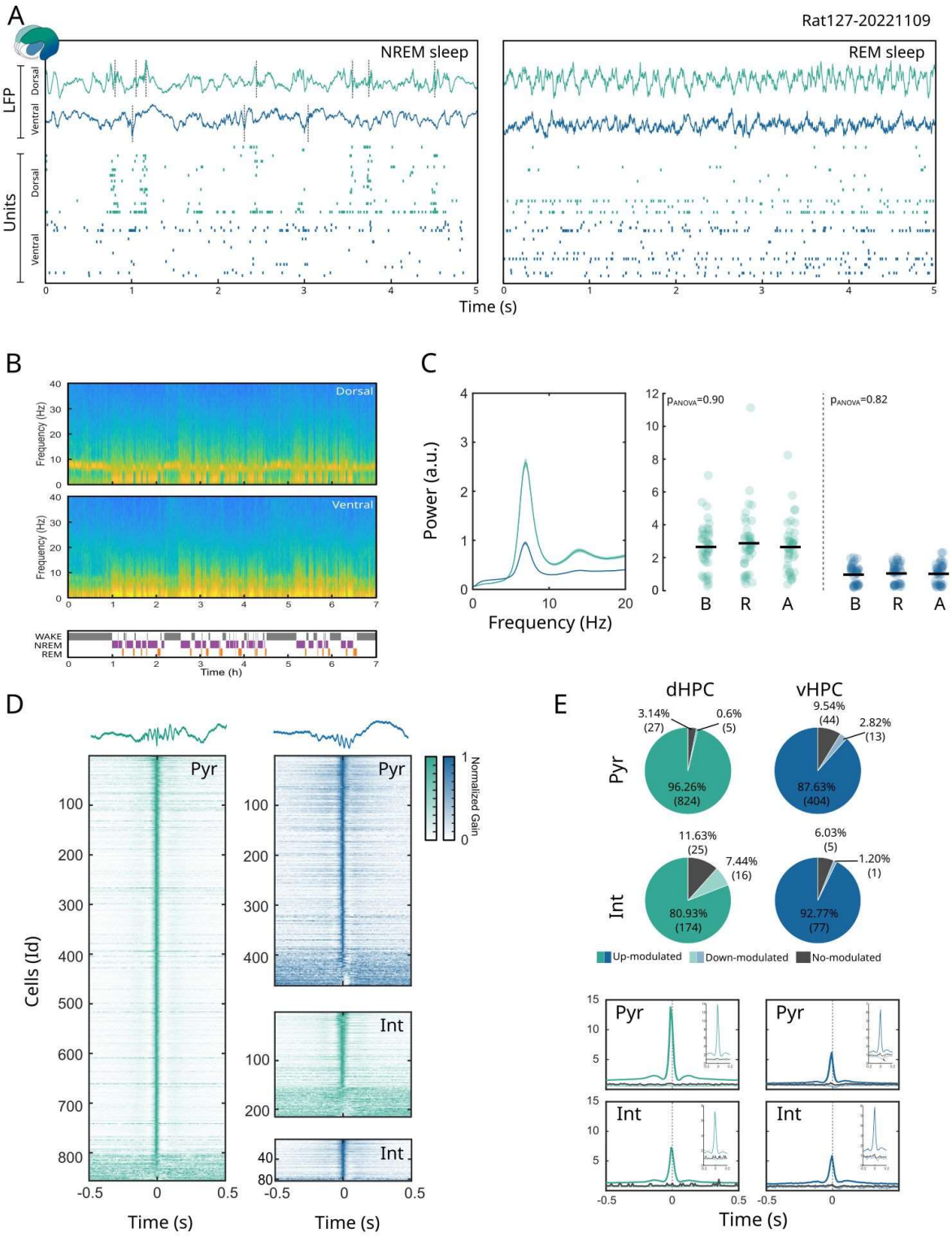


**Supplementary Figure 5: Sleep characterization in dorsal and ventral hippocampus**. (A) After spike sorting and ripple detection (marked with dashed lines), we differentiated between awake, NREM (left panel), and REM (right) sleep epochs. (B)To do so, we used the theta/delta ratio and the motion signal coming from the accelerometer. (C) Power spectrogram from dorsal (in green) and ventral (in blue) hippocampus. Right panel, power spectrum maximum value detected in theta band (6-10 Hz) across baseline, reward, and aversive sleep sessions (B, R, A respectively). One-way ANOVA, $N_{dHPC}$=40, $N_{vHPC}$=47. (D) Normalized peri-event gain of dorsal (in green) and ventral (in blue) pyr- and interneurons to local ripple events. (E) Using a Poisson test, we classified single units that were up-, down-, or non-modulated during the ripples. Upper panel, percentages of units across categories. Lower panel, the Average gain of units responds separating them using their response to the ripples.

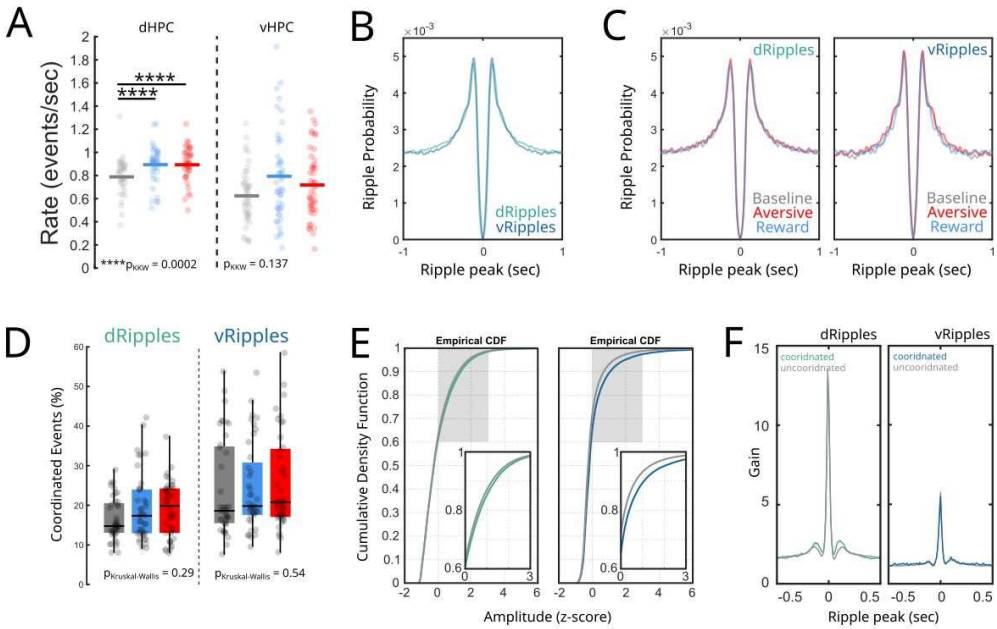


**Supplementary Figure 6: Characterization of dorsal-ventral ripple coordination**. (A) The ripple rate was calculated in both structures across emotional conditions. Only the dHPC ripple rate was increased in both emotional conditions compared to baseline sleep. Kruskal-Wallis test, ****p<0.0001, post-hoc test ****p<0.0001. (B) Autocorrelograms of dorsal and ventral ripple peaks detected in all sleep epochs, and (C) separating them between emotional conditions. (D) Percentage of coordinated events across emotional conditions. Kruskal-Wallis test. (E) Ripple peak amplitude is represented in a cumulative plot for coordinated (in green and blue) and uncoordinated ripples (in gray). Note that coordinated events showed higher amplitude compared to uncoordinated ones. (F) Gain peri-event histogram of pyr single unites locked to coordinated and uncoordinated dorsal (left panel) and ventral (right panel) ripples.

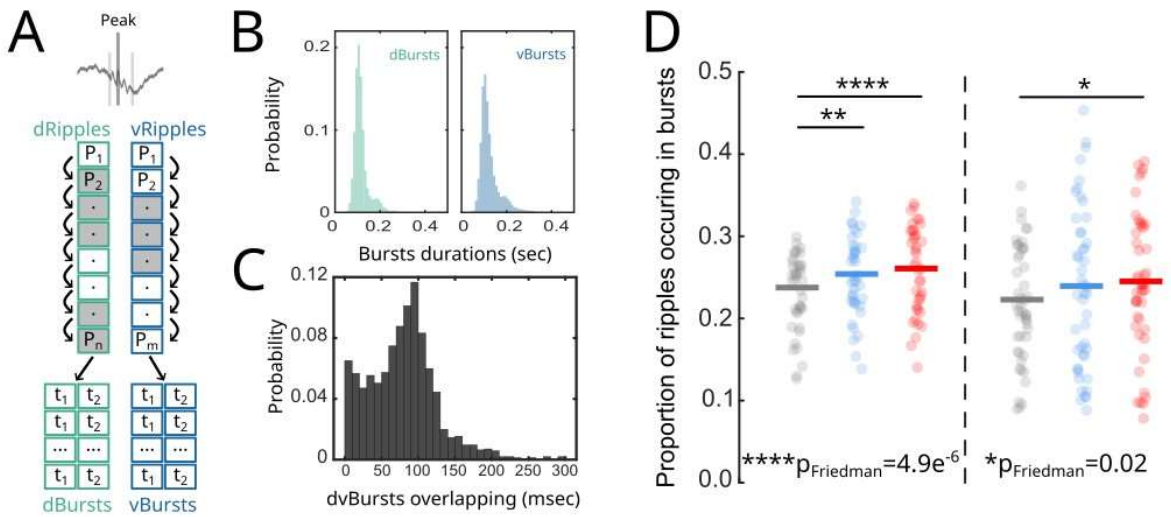


**Supplementary Figure 7: Ripple bursts characterization**. We defined a ripple burst to all subsequent ripples with <100 ms between each other. (A) Schematic representation of the method we used to detect ripple bursts. (B) Histogram of dorsal and ventral ripple bursts. (C) Histogram of dorsal-ventral bursts overlapping. Friedman test, followed by Tukey-Kramer post-hoc test, *p<0.05, **p<0.01, ****p<0.0001, $N_{dHPC}$=40, $N_{vHPC}$=47.

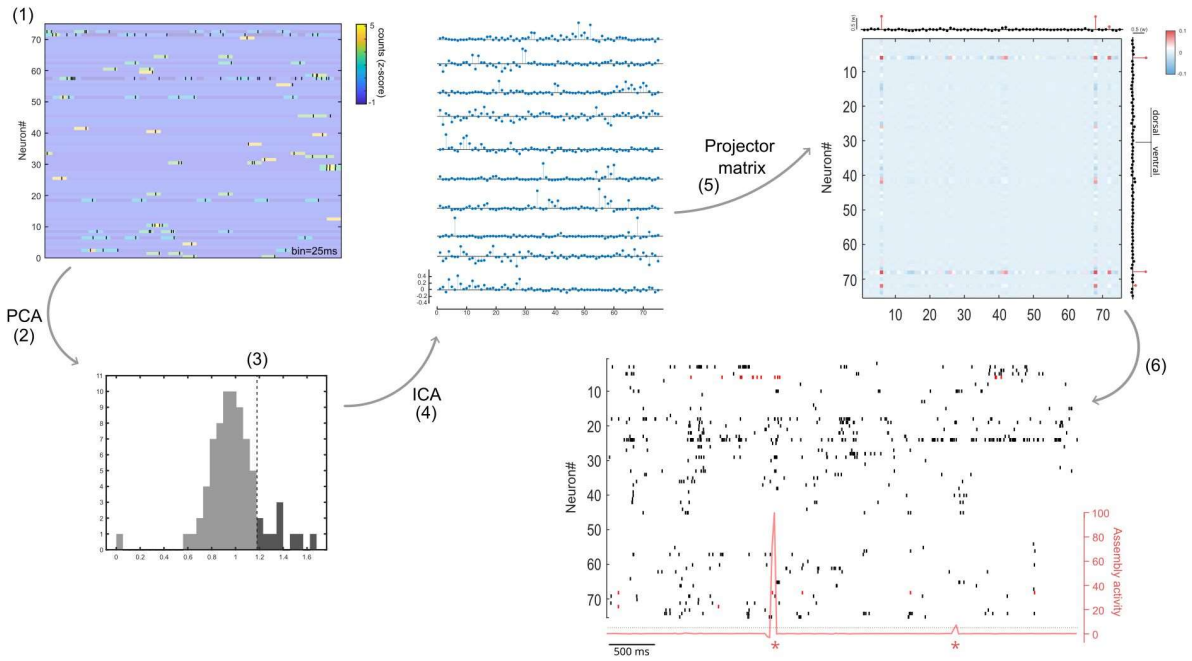


**Supplementary Figure 8: Schematic of the procedure for assembly pattern identification**. The procedure was performed using putative-pyr units coming from both: the dorsal and ventral hippocampus. After constructing the spike trains (25ms time bins) and z-scored them (1), a principal component analysis (PCA, 2) was performed. To identify the patterns describing significant co-activations between units, the Marcenko-Pastur threshold was applied (3). Independent component analysis (ICA, 4) was subsequently applied to identify assembly patterns that were above the threshold applied in step 3. To track the assembly pattern activation, a projector matrix was constructed by doing the outer product of the weight vector and setting the matrix diagonal to zero (5). The assembly activation strength was calculated as the quadratic form of the projector matrix with the convolved and z-scored spike trains (6).

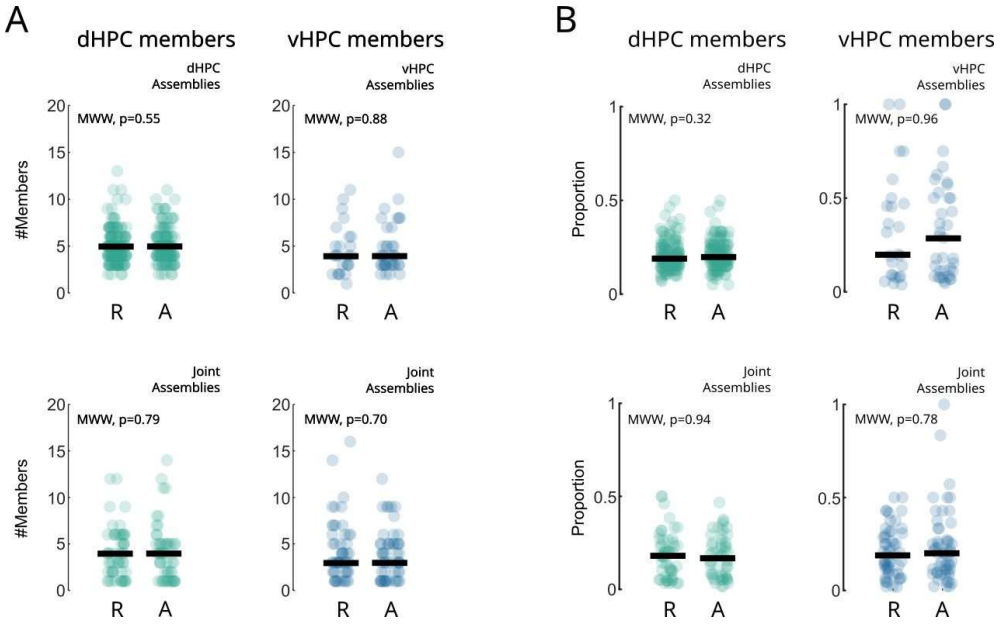


**Supplementary Figure 9: Members quantity after thresholding assemblies weight vectors**. Assemblies members were defined as those units whose ICA weight exceeded a threshold defined as the absolute value of $1/N_{units}$. (A) Number of dorsal (right panel) and ventral (left panel) members across dorsal, ventral (upper panel), and joint assemblies (lower panel) detected during rewarded or aversive runs (R or A respectively). (B) Proportion of members to the total number of recorded units during the session. No significant difference was observed between aversive and reward assemblies. Mann-Whitney test.

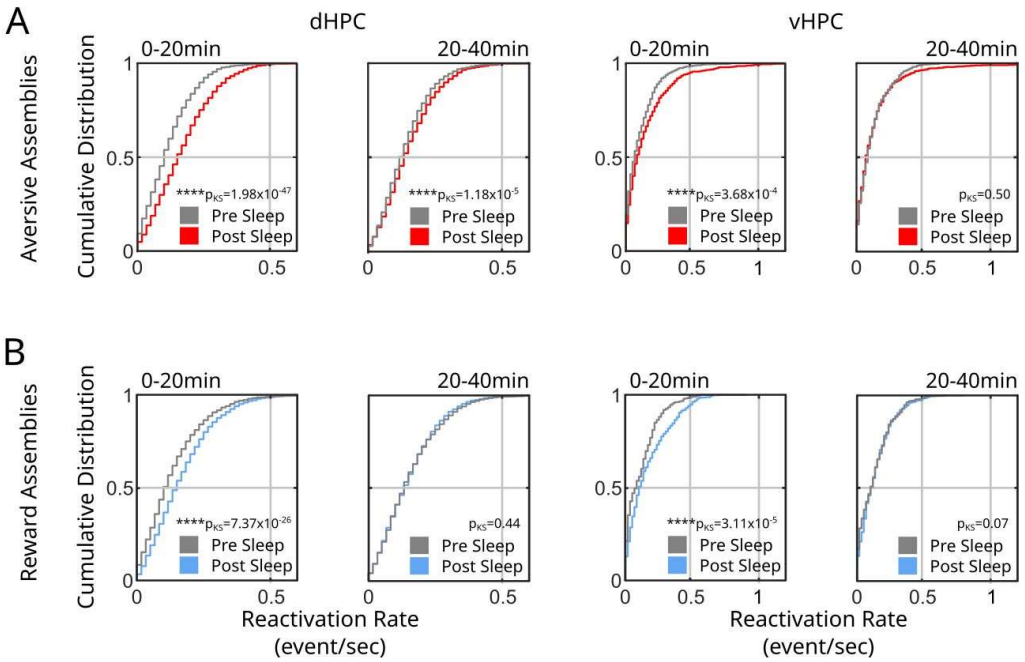


**Supplementary Figure 10: Reactivation rate in dorsal and ventral assemblies**. Assemblies reactivation rate across time during pre- and post-sleep sessions. The reactivation rate was calculated in 60-second bins aversive (A) and rewarded (B) assemblies' activity. In both: dHPC and vHPC assemblies, the reactivation rate was significantly higher at the beginning of the post-sleep session and progressively went back to pre-sleep levels at later time bins. Kolmogórov-Smirnov test, ****$p<0.0001$. Aversive assemblies, $N_{dHPC}=131$, $N_{vHPC}=37$; Reward assemblies, $N_{dHPC}=146$, $N_{vHPC}=25$.

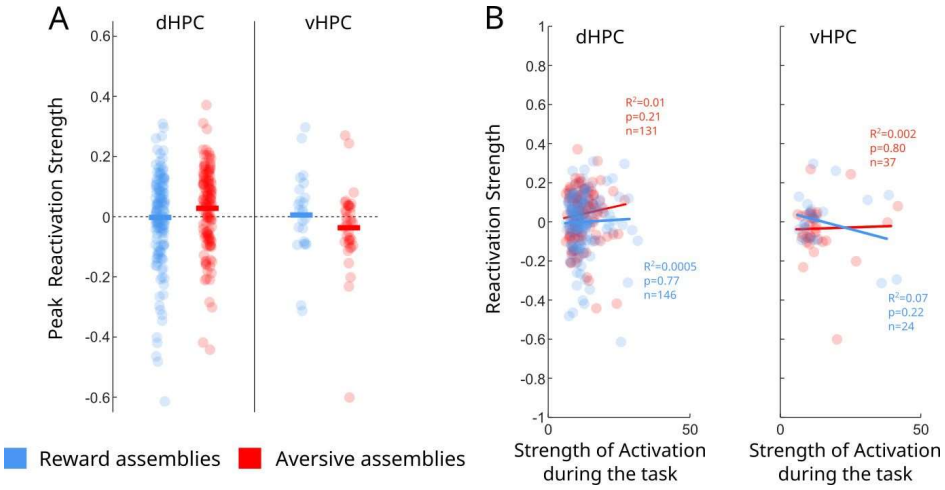


**Supplementary Figure 11: Peak Reactivation Strength for dorsal and ventral assemblies detected in both emotional conditions**. Peak Reactivation Strength was calculated as the average of the peak value from the post-sleep minus those coming from the pre-sleep divided by the peak value average from both sleep sessions. Wilcoxon test, p>0.05. (D) Linear correlation between the Peak Reactivation Strength and Activation Strength during the task. Linear regression, p>0.05. Aversive assemblies, $N_{dHPC}$=131, $N_{vHPC}$=37; Reward assemblies, $N_{dHPC}$ =146, $N_{vHPC}$=25.

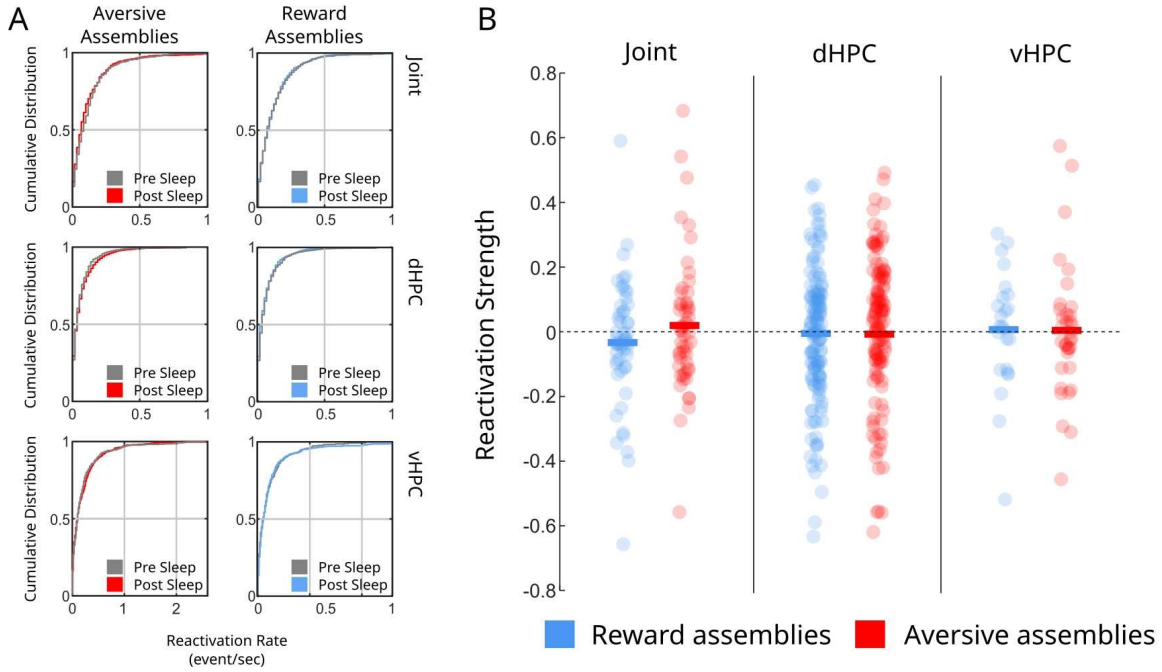


**Supplementary Figure 12: Assembly reactivation during REM sleep**. (A) Assemblies reactivation rate across time during pre- and post-sleep sessions. The reactivation rate was calculated in 60-second bins for aversive and rewarded assemblies (joint: upper, dHPC: middle, vHPC: lower). No differences between Post and Pre-sleep were observed. Kolmogórov-Smirnov test. (B) Peak Reactivation Strength was calculated for all types of assemblies. Wilcoxon test against zero, $p>0.05$. Aversive assemblies, $N_{dHPC}=131$, $N_{vHPC}=37$; Reward assemblies, $N_{dHPC}=146$, $N_{vHPC}=25$.

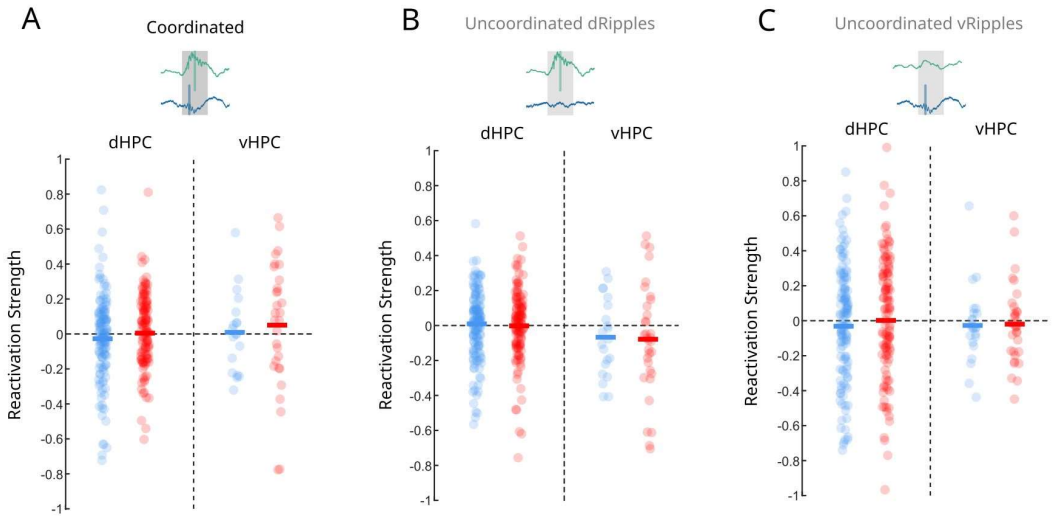


**Supplementary Figure 13: Peak Reactivation Strength from dorsal and ventral assemblies was not increased during coordinated and uncoordinated ripples.** Peak Reactivation Strength of dorsal and ventral assemblies during (A) coordinated and uncoordinated (B) dorsal, and (C) ventral ripples. Wilcoxon signed rank against zero.